Electronic Supplementary Information (ESI)

Perfect blackbody sheets from nano-precision microtextured elastomers for light and thermal radiation management

Kuniaki Amemiya,[a,*] Hiroshi Koshikawa,[b] Masatoshi Imbe,[a] Tetsuya Yamaki,[b]

and Hiroshi Shitomi [a]

[a] National Metrology Institute of Japan (NMIJ), National Institute of Advanced Industrial Science and Technology (AIST), 1-1-1 Umezono, Tsukuba, Ibaraki 305-8563, Japan

[b] Takasaki Advanced Radiation Research Institute, National Institutes for Quantum and Radiological Science and Technology (QST), 1233 Watanuki, Takasaki, Gunma, 370-1292, Japan

Corresponding Author

*E-mail: k.amemiya@aist.go.jp (Kuniaki Amemiya)

Finite differential time domain simulation. Numerical simulations of spectral reflectance were conducted by using the finite differential time domain (FDTD) software of MEEP[1] from Massachusetts Institute of Technology, USA. The MEEP software requires the dielectric function of the target material $\varepsilon(\omega)$ expressed by Lorentz's model:

$$\varepsilon(\omega) = \varepsilon_\infty + \sum_n \frac{\sigma_n \omega_n^2}{\omega_n^2 - \omega^2 - i\omega\gamma_n},$$

where ε_∞, ω_n, γ_n and σ_n are the dielectric constant of infinite-frequency limit, the n-th resonant optical angular frequency, the corresponding damping constant, and the oscillator strength of the target material, respectively. For PDMS, the documented Lorentz's parameters ε_{PDMS} of ref.[2] were used in our simulation. A geometry model of a conical spike or pit (Fig. S1a) having opening diameters d (=2r) of 2, 4 or 10 μm and aspect ratio h/r of 1, 3 or 5 was built, where h denotes the height of the spike or depth of the pit. Then, normal-incidence hemispherical reflectance spectra, which includes specular and all diffusive reflectance, were calculated for mainly mid-infrared wavelengths (4–15 μm). For simplicity, the simulation was conducted for a single unit cell having only one micro-cavity (spike or pit) in it but under Bloch-periodic boundary conditions (Fig. S1a). The sample thickness was assumed to be infinity, and, therefore, the effect of back reflection at an actual sample bottom was not fully considered.

For CR-39 or UV resin, the numerical simulation was not conducted, owing to the lack of reported Lorentz's parameters. Nevertheless, comparable results are expected because the averaged Fresnel reflectances of the untextured CR-39, UV resin, and PDMS were similar to each other, which means they have a similar refractive index at mid-infrared wavelengths. For the mixture of PDMS and carbon black of 5% by weight, the Lorentz's parameters of graphite $\varepsilon_{G\perp}$ in ref.[3] were also used with an effective medium theory: $\varepsilon_{mixture} = (1\text{-}f)\cdot\varepsilon_{PDMS} + f\cdot\varepsilon_{G\perp}$, where f denotes the concentration of the carbon black (f=0.05).

To avoid a plot error in logarithmic graphs, sub-zero reflectance data caused by the numerical instability were replaced by pseudo positive small values of 10^{-8} (Fig. S1b–d).

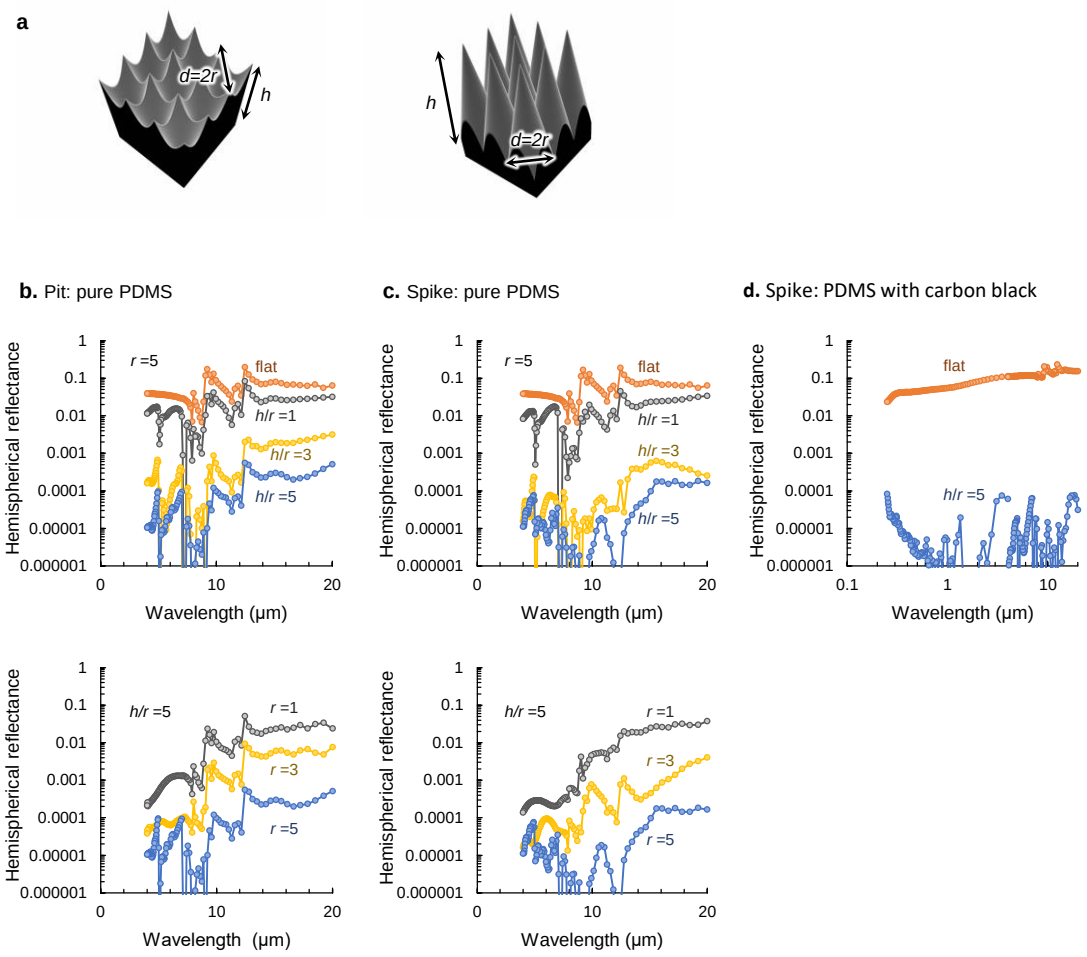

Fig. S1 Numerical simulation of the micro-cavity blackbody performance.

a) A simulation geometry of pit- (corresponding to master mould or positive replica) and spike-type (corresponding to negative replica) micro-cavities. b), c) Simulated reflectance spectra of PDMS micro-cavity blackbodies. Dependence of pit aspect ratio with fixed opening diameter d (=2r) of 10 μm (upper row), and dependence of opening diameter with fixed aspect ratio h/r of 5 (lower row) for pit- (b) and spike-type cavities (c). Comparable results are expected for CR-39 or UV resin as well. d) Simulation results for a PDMS micro-cavity blackbody with carbon black filler.

Optical characterization (see also Experimental section in main text). The measurement of ultralow reflectance requires special care; we conducted the measurement according to the guide of ref.[4]. In particular, the measurement system's (1) throughput, (2) baseline signal and (3) response linearity had to be considered in detail.

(1) *Throughput.* The sample reflectance ($\lesssim$0.001) is significantly lower than the reference reflectance (~0.9). In this case, exchanging the sample and the reference on a single measurement port largely changes the throughput of the integrating sphere, resulting in an underestimate of the sample reflectance (factor ~0.6, at worst, in our system). To avoid this throughput fluctuation, we used an integrating sphere having two sample ports: the low-reflectance sample was set on one port, and the reference on the other port (Fig. S2a). An infrared beam introduced into the integrating sphere was flipped by the mirror and directed to each measurement port. This setup can maintain the system throughput during the measurement, preventing underestimation of the sample reflectance.

(2) *Baseline signal subtraction.* The flipping mirror inside the integration sphere partially scatters the incident infrared beam, causing slightly overfilled illumination onto the sample port. Therefore, even if the sample port is empty, the non-negligible baseline signal is measured. To determine the net reflectance of the samples, we subtracted this baseline spectrum from the raw sample spectrum (Fig. S2b). In this case, the detector noise sometimes caused sub-zero reflectance data in the net reflectance spectrum. To avoid a plot error in logarithmic graphs, the sub-zero data were replaced by pseudo positive small values of 10^{-8} (Fig. 2f, Fig. 3e–g, Fig. 5b and Fig. S2b (right)). Note that we made no correction on the baseline signal in terms of the system's throughput fluctuation. Regardless of whether the low reflectance sample is on the sample port or not, the system's throughput was maintained within relatively 3.5% at worst (typically <0.5%). This contribution to measurement uncertainty was estimated as relatively 2%. In the absolute scale, at 10 μm in wavelength, for example, the uncertainty was 0.00004 for the baseline signal of 0.002 reflectance-equivalent.

The light which exits the Sample port 1 is directed to the ceiling of our laboratory. There would be little risk to detect the signal from undesired back-reflection for light which exits the Sample port 1 and eventually strikes another surface. Indeed, we measured the baseline signal with a

mid-infrared opaque plate (PMMA) placed at several tens of centimetres above the Sample port 1 and confirmed that the baseline signals were reproduced within the standard deviation of ~0.0003. We also measured the zero-input signal with the Sample port 1 open and confirmed no significant signal obtained.

(3) *Response linearity.* The system's response linearity may also affect the measurement results because the signal level for the low-reflectance sample is more than three orders of magnitude different from the reference reflectance. Mercury cadmium telluride detectors are known to show a linear response within relatively several-percent deviation over three decades of dynamic range.[5,6] The nonlinear deviation is caused by detector saturation at the high signal level, and therefore, there is little risk to underestimate the signal of low reflectance level. To briefly check our system's linearity, a neutral density (ND) filter from germanium (50% or 10% nominal transmittance) was placed in the input optical path, and it was confirmed whether the resultant signal attenuation was maintained at several different signal levels. Fig. S2c shows the transmission spectra of the ND filters measured at signal levels from 0.002 to 1 reflectance-equivalent. At any signal levels, we confirmed nearly identical signal attenuation for a single fixed-transmittance ND filter, suggesting that the system had a close-linear response. The noisy deviations at shorter or longer ends of wavelength (<6 μm or >10 μm) are attributable to the low responsivity of the detector. The error owing to the system's linearity was conservatively estimated as relatively ~10% at worst, corresponding to the standard uncertainty of relatively 5.8%.

Measurement uncertainty and validation. Other uncertainty factors, as follows, were also estimated according to 'Guides to the expression of uncertainty in measurement' (GUM);[7] the measurement uncertainty owing to the reference reflectance from Infragold; the system's drift; measurement repeatability were estimated as relatively ~2.6%; relatively ~5.8%; and absolutely 0.0001–0.0008 reflectance-equivalent (depending on wavelength), respectively. By combining all the above uncertainty contribution, we estimated the reflectance measurement uncertainty as absolutely ~0.0005 at 95% confidence level, for the reflectance of 0.0005 at 10 μm in wavelength. The uncertainty budget is summarized in Table S1, and the example of uncertainty spectrum is plotted in Fig. S2b (right). The uncertainty budget (Table S1) may not be exhaustive: we included FTIR-related sources of error, that is, the system's linearity and drift, but we did not

fully discuss the effects of Fourier transform (FT) processing. Nevertheless, considering the earlier reports on the uncertainty analyses of FTIR measurements,[8,9] the FT processing would hardly cause as large uncertainty as relatively several percents. Therefore, the combined uncertainty in Table S1 would not be too much underestimated.

The measured reflectance was partially validated by comparison between the FTIR and UV-NIR spectrophotometer at an overlapped wavelength of approximately 2 μm. Their results for the same samples agreed within the uncertainty, as shown in Fig. 5b.

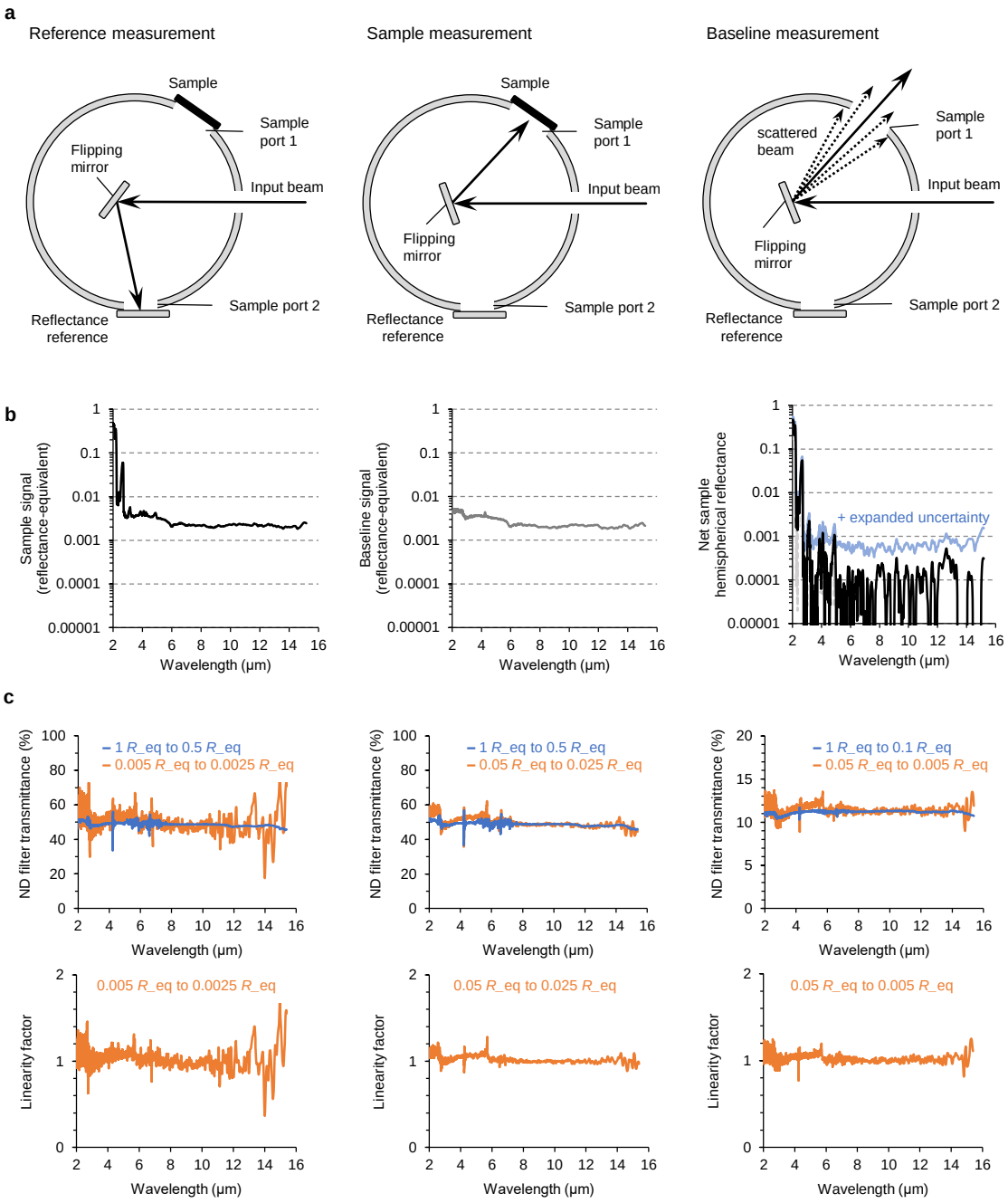

Fig. S2 FTIR measurement of hemispherical reflectance.

a) Setup of the integrating sphere of FTIR used in this study. A low-reflectance sample and a reference reflectance standard were placed at two separate ports of the integrating sphere (left, centre). Baseline signal was determined by emptying the sample port (right). b) Observed sample signal (left), baseline signal (centre) and net hemispherical reflectance spectrum for the

microtextured CR-39 plate (Fig. 2b) with the uncertainty of 95% confidence level (right). c) The system's nonlinearity estimation via transmittance measurements of ND filters at several signal levels. The nominal transmittances of the ND filters were 50% (left, centre) and 10% (right). The linearity factor is defined as the ratio of the measured transmittances: a close-unity linearity factor implies that the system has a linear response. *R*_eq, reflectance equivalent.

Table S1 Uncertainty budget of hemispherical reflectance measurement.

Component	Standard uncertainty	Unit	Type	
Reference reflectance standard	2.6	%	B	Relative
FTIR system				
Baseline	2.0	%	B	Relative
Linearity	5.8	%	B	Relative
Drift	5.8	%	B	Relative
Measurement repeatability	0.0001–0.0008[a)]		A	Absolute
Combined standard uncertainty	0.00023[b)]			Absolute
Expanded uncertainty (95% confidence level)	0.0005[b)]			Absolute

[a)]Depending on the wavelength
[b)]Examples for the reflectance of 0.0005 at 10 μm in wavelength

Fabrication of nickel metal replica. For nickel metal replication, electroforming was conducted by Kiyokawa Plating Industry, Co., Ltd., Japan. One of the micro-cavity templates was coated with titanium and copper of 50 nm and 300 nm in thickness as an electrode used in electroforming. Nickel electroplating was then conducted (plating thickness was 500 μm), and, after that, the nickel metal replica was peeled off from the template.

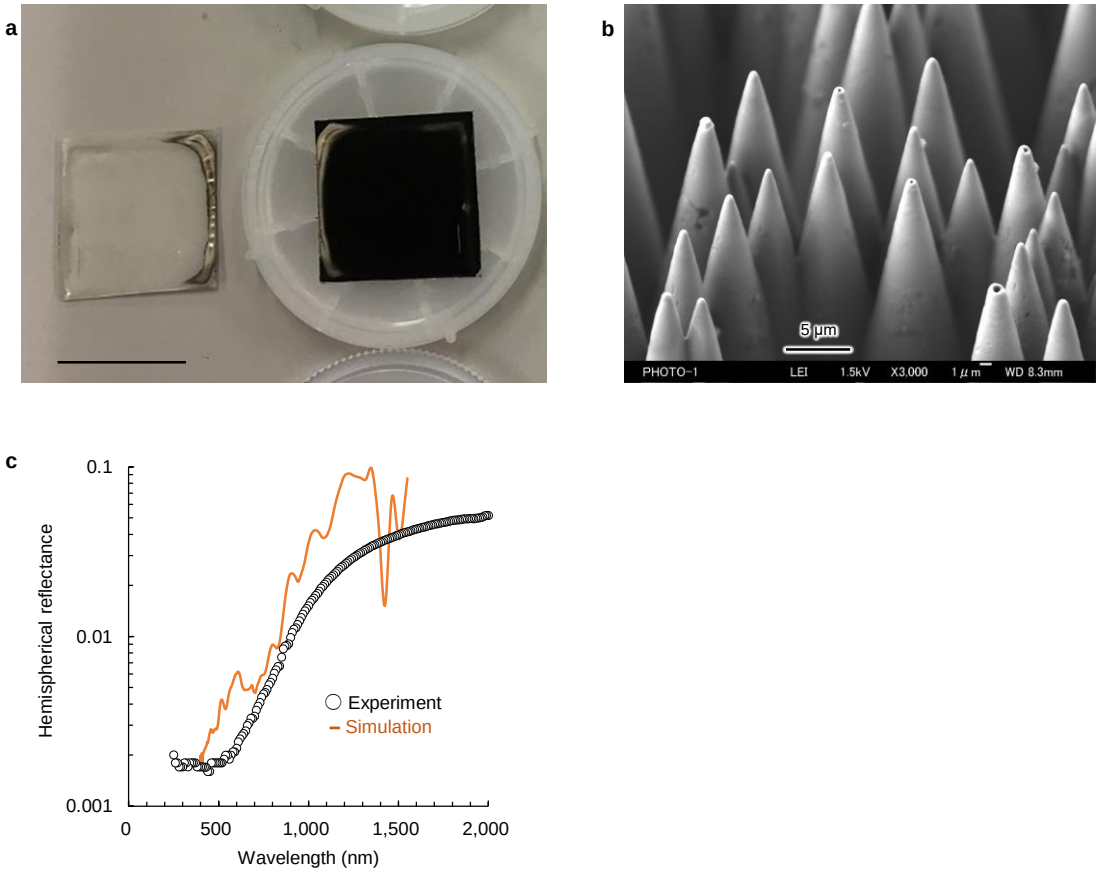

Fig. S3 Stamp mould from nickel electroforming.

a) The nickel electroformed stamp mould (right) replicated from the microtextured CR-39 master mould (left). Scale bar, 20 mm. b) SEM image of the stamp mould from nickel electroforming. c) The hemispherical reflectance of the stamp mould acquired with a UV-NIR spectrophotometer (open symbols). Despite the metallic composition, the stamp mould exhibited low-reflectance (0.002–0.005) black appearance in the visible regime, as expected in the numerical simulation (orange solid line).

Restoring the collapsed micro-cavities. Exposure to solvent of high surface tension, such as water, can lead to degradation of the PDMS micro-cavities—paring of the textures. To restore the texture, immersion in 1% sodium dodecyl sulphate solution and a subsequent rinse in heptane were conducted[10] under ultrasonication for approximately two minutes. Note that heptane solvent strongly swells PDMS sheets, and, therefore, overnight drying was necessary to restore the sheets to their original state.

Thermal shock test. Stability against cold shocking was tested by putting the PDMS blackbody sheet into liquid nitrogen until boiling finished on a plastic case (Fig. S4b). Heat resistance was tested by heating up to ~190 °C on a hot plate (Fig. S4c). After each testing procedure, the spectral reflectance of the sample was measured again and compared with that prior to the test.

Thermal conductivity of blackbody sheets. In the case of precision blackbody applications such as planar standard radiators or blackbody tapes, temperature gradient that might occur between the top and the bottom of a sheet is also key issue. A simple model, considering only thermal loss from convection on the top surface in air, suggests that thermal conductivity of >1 $Wm^{-1}K^{-1}$ is necessary for 500 μm thick sheet to achieve desirable top-bottom temperature deference of <0.1 °C at ambient temperature. Elastomers including PDMS have low thermal conductivity of ~0.2 $Wm^{-1}K^{-1}$, however, pre-addition of thermal conductive filler into PDMS prepolymer would address this issue.

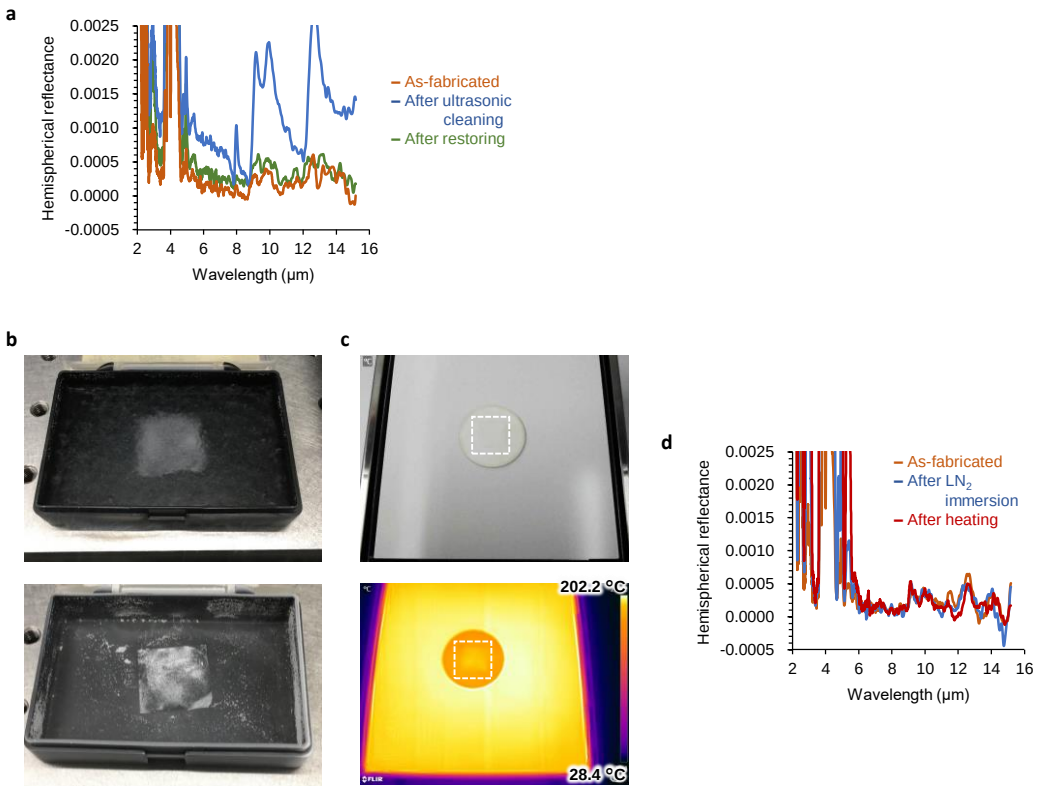

Fig. S4 Testing for ultrasonic cleaning and restoring, and thermal shock.

a) Ultrasonic cleaning in water degraded the PDMS positive replica, resulting in increased reflectance, whereas exposure to 1% sodium dodecyl sulphate solution with the following heptane rinse completely restored the original ultralow reflectance. b) Cold shock (immersion in liquid nitrogen) and c) heating up to ~190 °C on a hot plate hardly changed the ultralow reflectance of the micro-cavity blackbody sheets from PDMS positive replica (d). Dashed-line squares in c) denote the position where the PDMS blackbody sheet was placed.

References

1 A. F. Oskooi, D. Roundy, M. Ibanescu, P. Bermel, J. D. Joannopoulos and S. G. Johnson, *Comput. Phys. Commun.*, 2010, **181**, 687–702.

2 A. Srinivasan, B. Czapla, J. Mayo and A. Narayanaswamy, *Appl. Phys. Lett.*, 2016, **109**, 061905.

3 E. Lidorikis and A. C. Ferrari, *ACS Nano*, 2009, **3**, 1238–1248.

4 J. Lehman, C. Yung, N. Tomlin, D. Conklin and M. Stephens, *Appl. Phys. Rev.*, 2018, **5**, 011103.

5 E. Theocharous, J. Ishii and N. P. Fox, *Appl. Opt.*, 2004, **43**, 4182–4188.

6 E. Theocharous, *Metrologia*, 2012, **49**, S99–S104.

7 Joint Committee for Guides in Metrology (JCGM). Evaluation of Measurement Data—Guide to the Expression of Uncertainty in Measurement. *JCGM 100:2008*, 2008.

8 S. G. Kaplan, L. M. Hanssen and R. U. Datla, *Appl. Opt.*, 1997, **36**, 8896–8908.

9 L. Hanssen, *Appl. Opt.*, 2001, **40**, 3196–3204.

10 E. Delamarche, H. Schmid, B. Michel and H. Biebuyck, *Adv. Mater.*, 1997, **9**, 741–746.